Thermochimica Acta 507–508 (2010) 15–20

Contents lists available at ScienceDirect

Thermochimica Acta

journal homepage: www.elsevier.com/locate/tca

Heat transfer in salt solutions enclosed in DSC cells

A. Jamil[a], T. Kousksou[b,*], K. El Omari[b], Y. Zeraouli[b], Y. Le Guer[b]

[a] École Supérieure de Technologie de Fès, Université Sidi Mohamed Ibn Abdelah, Route d'Imouzzer BP 2427, France
[b] Laboratoire de Thermique Energétique et Procédés, Université de Pau et des Pays de l'Adour (UPPA), Campus Universitaire, 64000 Pau, France

ARTICLE INFO

Article history:
Received 20 February 2010
Received in revised form 21 April 2010
Accepted 29 April 2010
Available online 6 May 2010

Keywords:
Entropy generation
Thermodynamics
Phase change
Salt solutions
DSC

ABSTRACT

This study addresses the heat transfer in differential scanning calorimetry (DSC) cells during the melting process of an eutectic solution. The energy and entropy equations for two-dimensional transient thermal analysis with associated boundary and initial conditions are solved numerically using a fixed grid numerical model with the finite control volume approach. Proper trends and a good agreement between the results of theoretical modeling and experiment results are obtained. A parametric study with various associated parameters is performed and results are illustrated.

1. Introduction

Recently, latent heat thermal storage received particular attention in the literature due to the high storage density and the isothermal nature of the storage and removal processes [1]. The development history of latent storage systems is the development history of storage materials [2]. Among the most extensive references related with phase change materials (PCMs), one can cite Abhat [3], Lane [4], Garg et al. [5], Husnain [6], Dincer and Marc [7], Mohammed et al. [8], Felix Regin et al. [1] and Zalba et al. [9]. These contain a complete review of the type of materials that have been used, their classification, characteristics, advantages and disadvantages and the various experimental techniques used to determine the behavior of these materials during melting and solidification processes.

The PCMs are grouped into four categories, namely, organic, inorganic, fatty acids and commercial PCMs. Apart from the pure compounds, the eutectic mixtures can yield different phase change temperature. There is abundant information on PCMs in the literature. No material has all the optimal characteristics required for a PCM, and the selection of a PCM for a given application requires careful consideration of the properties of various substances. The design and operation of a latent heat thermal storage is dependent upon the physical and chemical characteristics of the PCM used [10]. The higher the energy density of the PCM, the smaller the necessary storage volume required for each proposed application. This implies a lower cost for the heat exchange structure or a greater total heat storage capacity of the system for the same overall volume. The reported results showed [1] that one cannot simply consider any available data on technical grade PCMs for designing an effective heat storage device, as thermophysical properties vary from manufacturer to manufacturer, mainly due to different level of impurities in technical grade PCMs.

The methods available for determining the heat of fusion, specific heat and melting point can be classified into three groups, namely, conventional calorimetry methods, differential scanning calorimetry methods and T-history method. The differential scanning calorimeter provides quick and reliable results in the form of energy–time diagrams (thermograms) using very small quantities of the sample (1–10 mg). Evaluation of the thermograms yields rather precise values of the phase transition temperatures during melting and freezing of sample, the heat of fusion and the specific heat variation as a function of temperature. The DSC method is well developed and a lot of researchers have used this method [11,12].

The objectives of this paper are to present a detailed analysis of the melting process of different eutectic solutions inside the DSC cell and to evaluate the entropy generation related to the phase change process using a fixed grid numerical model.

2. Binary eutectic phase diagram

Fig. 1 is an example of a salt binary eutectic phase diagram [13]. The liquidus line separates the salt solution phase from the ice–salt solution phase. The solidus line separates the ice–salt solution phase from the solid salt–ice phase. We note that the solidus and liquidus lines can be determined experimentally by melting

* Corresponding author.
E-mail address: Tarik.kousksou@univ-pau.fr (T. Kousksou).

0040-6031/$ – see front matter © 2010 Elsevier B.V. All rights reserved.
doi:10.1016/j.tca.2010.04.023

Nomenclature

c_p	specific heat capacity of the eutectic solution ($J\,kg^{-1}\,K^{-1}$)
c_R	specific heat capacity of the reference cell ($J\,kg^{-1}\,K^{-1}$)
ΔA	area (m^2)
ΔH	latent heat of ice melting ($J\,kg^{-1}$)
L_F	latent heat of fusion ($J\,kg^{-1}$)
L_D	heat of dissolution of salt in the solution of ice melting ($J\,kg^{-1}$)
M	mass (kg)
R	cell radius (m)
$\dot{S}'_{gen}$	entropy generation rate density ($W\,K^{-1}\,m^{-3}$)
t	time (s)
T	temperature (K)
T_E	eutectic temperature (K)
T_o	initial temperature (K)
$U_{1,2}$	heat transfer coefficient ($W\,m^{-2}\,K^{-1}$)
V	volume (m^3)
X	water concentration
X_E	eutectic concentration
Z	cell height (m)
Greek letters	
β	heating rate ($K\,min^{-1}$)
λ	heat conductivity ($W\,m^{-1}\,K^{-1}$)
ρ	density of the eutectic solution ($kg\,m^{-3}$)
ρ_{ic}	ice density ($kg\,m^{-3}$)
Φ	specific heat flow rate ($W\,kg^{-1}$)

and cooling samples of different compositions. These two lines cross at eutectic point (E) where can coexist the ice crystals, those of salt and the salt solution. The eutectic mixture has the lowest melting point (which is of course, the same as the freezing point) the temperature at which the eutectic mixture freezes or melts is known as the eutectic temperature T_E.

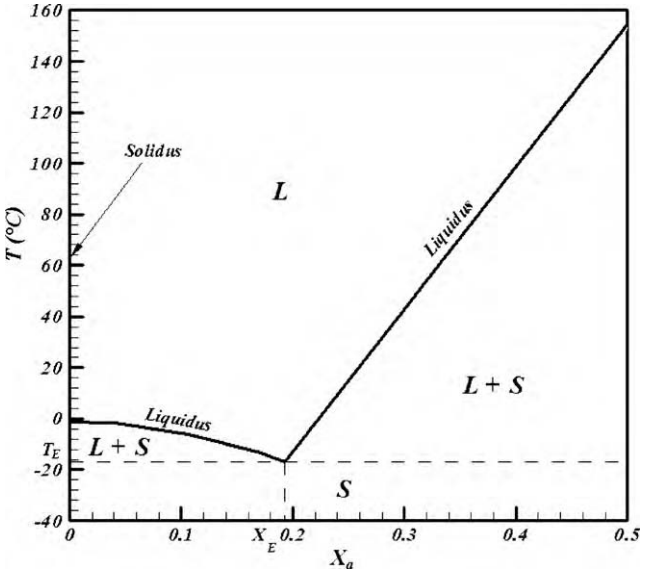

Fig. 1. Binary phase diagram NH_4Cl–H_2O [13].

Table 1
Eutectic solutions.

Salt solution	X_E	T_E
KCl–H_2O	0.197	262.55 K
NH_4Cl–H_2O	0.195	257.45 K
NaCl–H_2O	0.23	252.05 K

3. Experimental

Thermal analysis was carried out using a PYRIS DIAMOND DSC of PerkinElmer. The temperature scale of the instrument was carefully calibrated by the melting point of pure ice (273.15 K or 0 °C) and mercury (234.32 K or −38.82 °C). The principle of the power-compensation used in dispersed droplet is widely detailed in Refs. [14,15]. We have already presented the experimental cell in Ref. [14], which consists of a cylindrical cell of height $Z = 1.1$ mm and radius $R = 2.215$ mm.

The apparatus gives the specific heat flow rate Φ, the difference between the heat powers maintaining the plate supporting the active cell containing the eutectic solution and the plate supporting the reference cell:

$$\Phi = \Phi_{\text{active cell}} - \Phi_{\text{reference cell}} \quad (1)$$

As indicated in Ref. [14], the power exchanged at the reference plate is practically constant and equal to $\Phi_{\text{reference cell}} = \beta c_R$, where c_R is the specific heat capacity of the reference cell and β is the heating rate. So to simplify the model we will omit the second term from the calculation of Φ.

The DSC experiments were conducted by placing approximately 6–1 mg of each eutectic solution (Table 1) in a standard aluminum DSC sample pan. The sample was cooled at 5 °C/min from 4 °C, until ice nucleated in the solution (observed as a sharp negative peak on the DSC thermogram) typically between −30 °C and −40 °C. The sample was then re-equilibrated at this temperature for 3–5 min. Isothermal equilibrium at this temperature will permit the ice crystals to exist but not grow. The nucleated sample was then heated from −50 °C to 20 °C using different heating rates, to obtain the magnitude and the temperature dependence of the heat absorbed (i.e. the thermogram).

4. Physical model

4.1. Heat transfer analysis

For the proposed model, the following assumptions are made:

- The ice consists of pure water.
- The diphasic medium is considered as a binary mixture whose properties are given by combining properties of the liquid solution and those of pure ice.
- Due to the small dimensions of the sample, the convection effects due to density change at the phase change interface are neglected and salt concentration is uniform within the liquid solution fraction.

The model which we have adopted to describe the thermal transfers during the phase shift of the studied solution is based on an enthalpic formulation proposed by Voller and his co-workers [16,17]. This formulation rests on the partition of the volume occupied by the solution into a finite number of control volumes and the handwriting the energy conservation in cylindrical coordinates:

$$\rho c_p \frac{\partial T}{\partial t} = \lambda \left(\frac{\partial^2 T}{\partial r^2} + \frac{1}{r}\frac{\partial T}{\partial r} + \frac{\partial^2 T}{\partial z^2} \right) + \rho_{ic} \Delta H \frac{\partial X}{\partial t} \quad (2)$$

where ρ, c_p and λ indicate, respectively, the mass density, the specific heat capacity and the heat conductivity of the eutectic solution. X indicates the liquid fraction of water in the cell. The coefficient ΔH is given by:

$$\Delta H = L_F + \left(\frac{X_E}{1 - X_E}\right) L_D \tag{3}$$

where L_F and L_D represent, respectively, the latent heat of ice melting and the heat of dissolution of salt in the formed solution. X_E represents the eutectic concentration of the eutectic solution. During the melting process, the sample is regarded as a homogeneous material whose physical properties depend on the salt concentration and of the proportion of the ice which is melted.

To take into account the air between the solution and the cover of the cell, we consider two different heat exchange coefficients U_1 and U_2. So, the boundaries conditions are:

$$\left(\frac{\partial T}{\partial r}\right)_{r=0} = 0 \tag{4}$$

$$-\lambda\left(\frac{\partial T}{\partial r}\right)_{r=R} = U_2(T - T_{plt}) \tag{5}$$

$$-\lambda\left(\frac{\partial T}{\partial r}\right)_{z=0} = U_2(T - T_{plt}) \tag{6}$$

$$-\lambda\left(\frac{\partial T}{\partial r}\right)_{z=Z} = U_1(T - T_{plt}) \tag{7}$$

where T_{plt} is the plates temperature and it is programmed to be linear function.

$$T_{plt} = \beta t + T_0 \tag{8}$$

At $t = 0$ the initial conditions are $T(r, z, 0) = T_0$ and $T(r, z, 0) = 0$.

Because the thermal conductivity of air is smaller than that of the metal of the cell, we consider that all the energy is transmitted to the plate by the lower boundary of the cell. So, is the sum of the specific heat flow rate through the walls of the metallic cell:

$$\Phi = -\frac{1}{M}\sum_i U_i(T_i - T_{plt})\Delta A_i \tag{9}$$

where $U_i = U_1$ or U_2, M is the sample mass and ΔA is the area walls of the metallic cell.

The finite difference equations are obtained upon integrating Eq. (2) over each of the control volumes. The resulting finite difference scheme at the time $t + \Delta t$ has the following form:

$$a_P T_P = \sum_{nb} a_{nb} T_{nb} + \frac{\rho c_p V_p}{\Delta t} T_P^{old} + \rho_{ic}\Delta H \frac{V_p}{\Delta t}(X_p - X_P^{old}) \tag{10}$$

V_P is a volume associated with the Pth node point, the subscripts P, "nb(E,W,N,S)" and "old" refer to the Pth node point, the neighboring node points and the old time value, respectively. The calculation of the coefficients a_p and a_{nb} and the resolution of Eq. (10) are presented in Jamil et al. [18] and it is deemed to repeat it in the present work.

4.2. Entropy generation

The lost available work is directly proportional to the entropy generation in a nonequilibrium phenomenon of exchange of energy within the sample and at the solid boundaries. The local rate of entropy generation per unit volume in the cylindrical sample can be calculated using the following expression [19]:

$$\dot{S}'_{gen} = \frac{\lambda}{T^2}\left[\left(\frac{\partial T}{\partial r}\right)^2 + \left(\frac{\partial T}{\partial z}\right)^2\right] \tag{11}$$

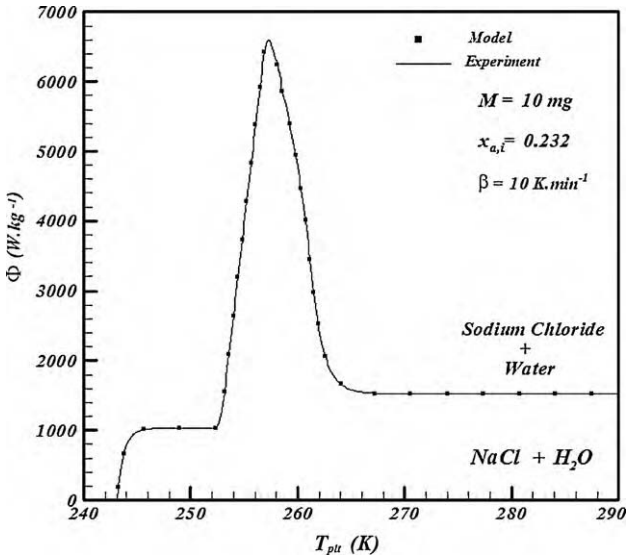

Fig. 2. Theoretical and experimental thermogram ($NaCl + H_2O$).

Entropy generation profiles may be constructed using Eq. (11) if the temperature profile is known in the heat transfer medium.

5. Results and discussion

The values of physical characteristics required in the different equations have been determined experimentally or taken in the literature [20–22], except the coefficients of heat exchange (U_1 and U_2) which have been determined by simulation from exploratory experiments.

In the case of an endothermic phase transition the heat consumption increases strongly and the sample temperature drops even more behind the program temperature. In the case of a first-order phase transition of an eutectic mixture, the sample temperature remains approximately constant until the phase transition of the sample is completed and then – following an exponential law – it relaxes to the temperature lagging only due to the heat capacity of the sample. During melting this leads to an endothermic DSC signal as depicted in Fig. 2. This figure shows an experimental thermogram for the melting of an eutectic solution ($KCl–H_2O$, $X_E = 0.197$, $T_E = -10.6\,^\circ C$), at $10\,^\circ C\,min^{-1}$, compared with the calculated thermogram obtained with the proposed model. The fit between the experimental and the calculated curve is good: the rounded form of the top of the peak is reproduced and its width is the same.

Fig. 3a–c shows the experimental and the numerical thermograms versus heating rates and for different eutectic solutions. The melting temperature range becomes broader and it shifts to greater temperatures with increasing heating rate. With the beginning of the transition (at T_E), the sample temperature remains constant, whereas the inert reference substance continues to be linearly heated. Thus, the difference temperature between sample and reference substance also increases linearly and reaches the maximum value and then drops again exponentially. While the 'extrapolated peak onset' of the transition characterizes the very beginning of melting at the crucible bottom, and therefore does not depend on sample size and transition heat but only on the heating rate and the heat transfer to the sample.

Fig. 4 presents the temperature of the eutectic solution at different point in the cell and the corresponding proportion of the ice which is melted X versus time. Important temperature differences can be observed as a function of the radius. Melting begins as soon as $T = T_E$ and it is very fast near the metallic boundaries and is slower

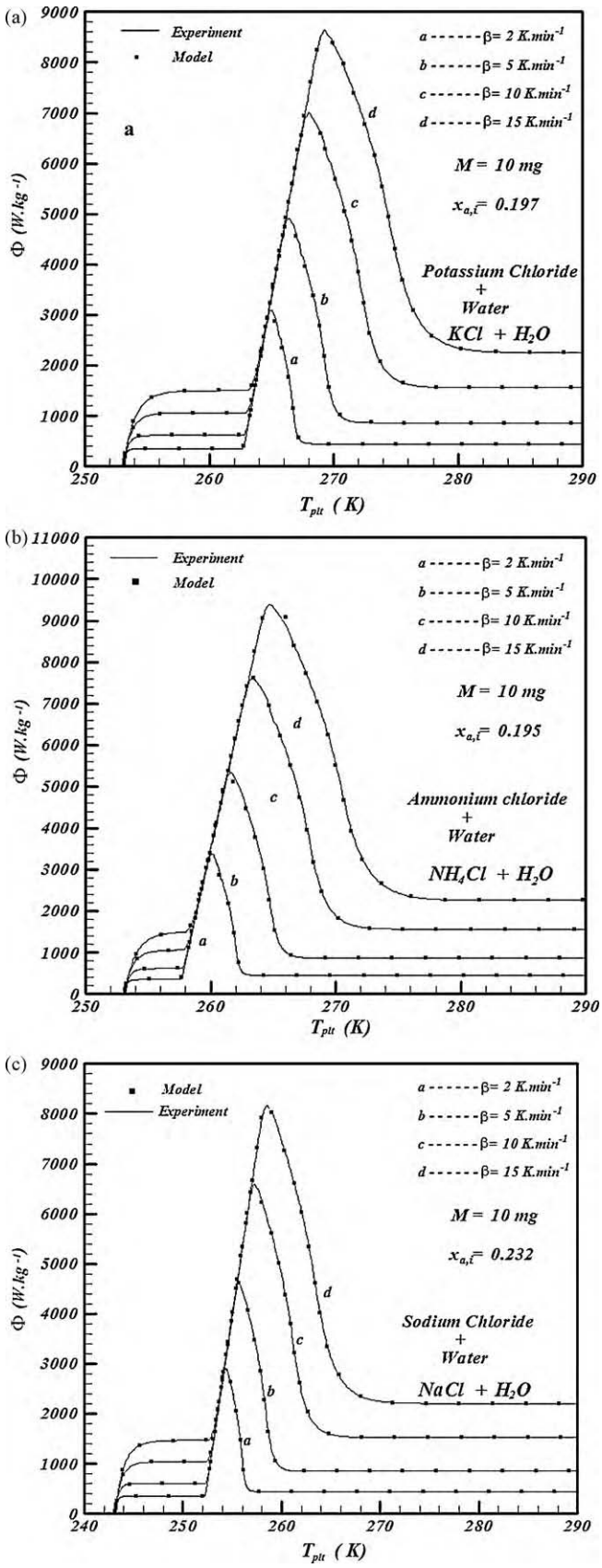

Fig. 3. (a) Effect of the heating rate on the shape of thermograms (KCl + H_2O). (b) Effect of the heating rate on the shape of thermograms ($NH_4Cl + HO_2$). (c) Effect of the heating rate on the shape of thermograms ($NaCl + HO_2$).

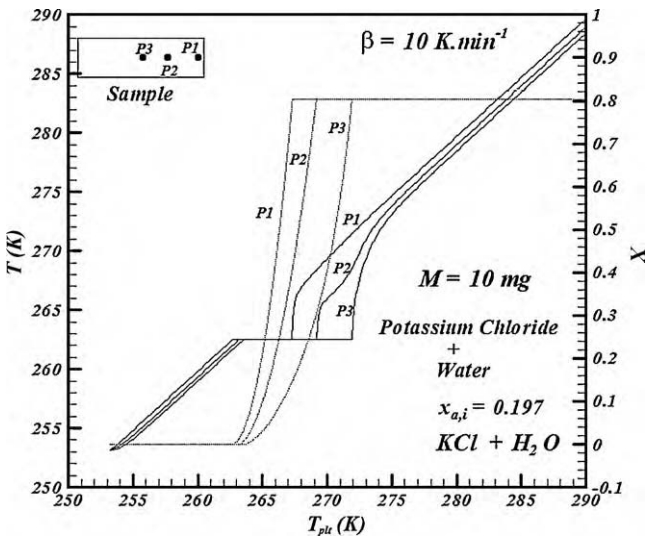

Fig. 4. Temperature and liquid fraction versus radius for $\beta = 10\,\mathrm{K\,min^{-1}}$.

in the central region. We can also note that, the temperature differences inside the DSC cell become more important as the heating rate increases (see Fig. 5a–c).

In Fig. 6, the relation between entropy generation and the plate temperature T_{plt} with different heating rates β is illustrated. Entropy generation rises with increasing heating rate. Fig. 7 shows the entropy generation versus the plate temperature for different cell masses. We note that an increase in the cell mass leads to an increase in the entropy generation inside the DSC cell. A chosen heating rate and an acceptable maximal temperature gradient inside the DSC cell induce a recommended sample mass. Analogous, a chosen sample mass and an acceptable maximal temperature deviation induce a recommended heating rate.

Increasing sample mass/size increases the thermal lag of sample temperature versus sensor temperature and in addition gives risk to temperature gradients within the sample resulting in peak broadening, while increasing the heating and cooling rates increases the thermal lag of the sensor temperature with respect to the furnace temperature. With the entropy generation theory, it is possible to predetermine the suitable protocol and thus to minimize the temperature gradient inside the sample.

5.1. Determining enthalpy change of melting process from DSC measurements

The enthalpy change of the phase transition process can be determined by DSC measurements. The area of a DSC peak can be used to estimate the enthalpy change of phase transition. The results from Figs. 8 and 9 indicate that the total enthalpy change ΔH via a complete phase change process is independent of DSC heating rate and sample mass, whereas the predicted enthalpy change during the melting process depends very much on the DSC rate and the sample mass. One explanation is that when the phase change process has not completed, any temperature change will lead to a latent heat change and the relation of latent heat change with temperature varies with the DSC rate and the sample mass. To evaluate the enthalpy change during the melting process, temperature gradient inside the PCM needs to be considered. For a given application that allows for charging/discharging of the storage in a certain temperature range, whether the storage density can reach the value of heat of fusion ΔH, depends on if the allowed temperature range is as large as the phase change temperature range. For designing a PCM thermal energy storage system, storage density and phase

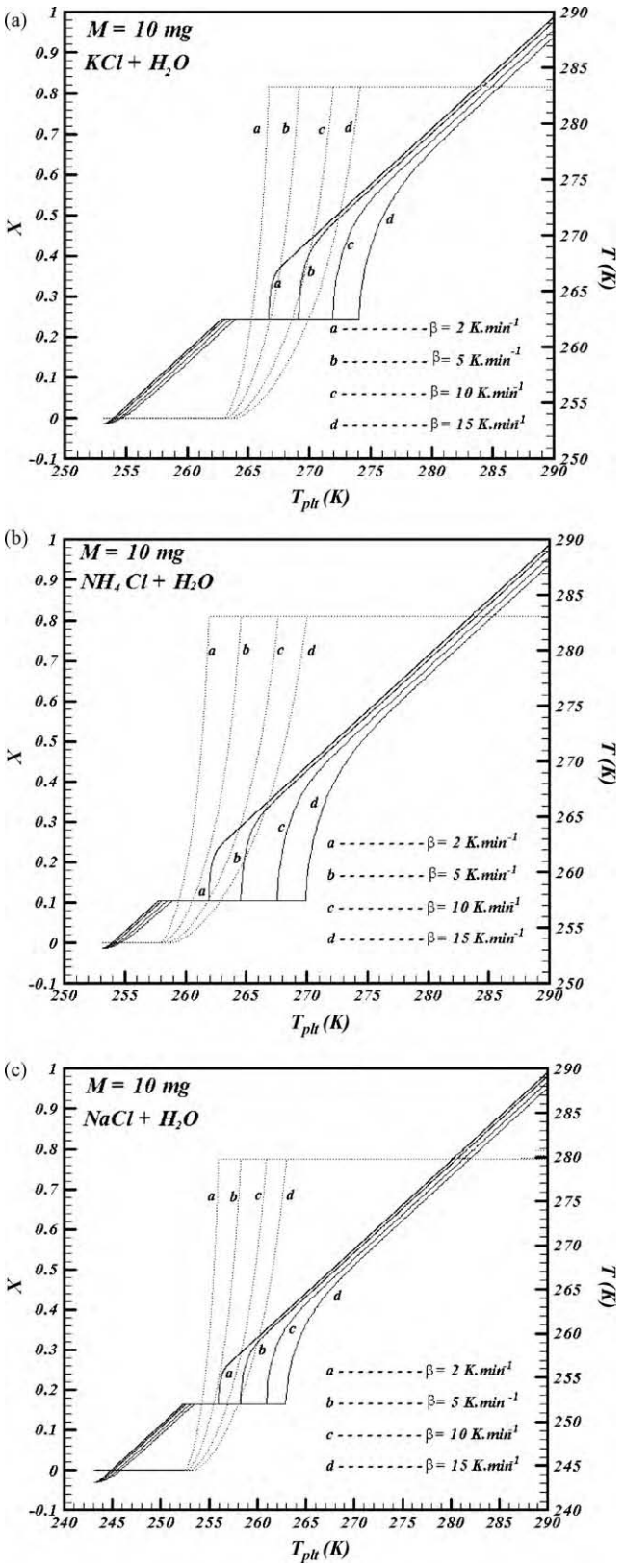

Fig. 5. (a) Influence of the heating rate on the temperature in the center of the sample; (b) influence of the heating rate on the temperature in the center of the sample; (c) influence of the heating rate on the temperature in the center of the sample.

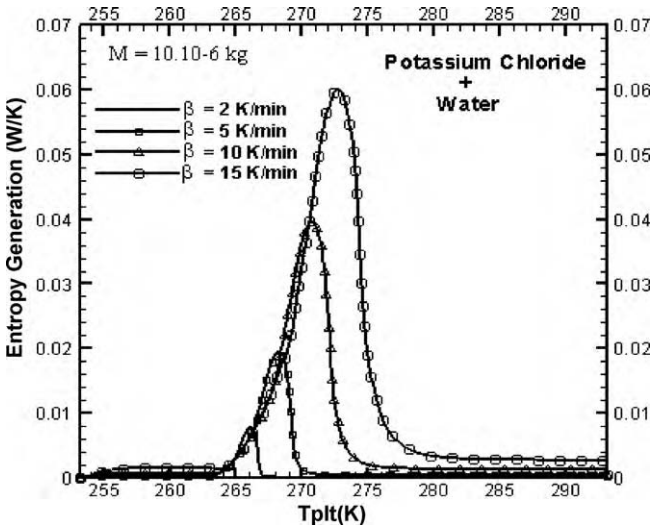

Fig. 6. Entropy generation versus T_{plt} for various heating rates.

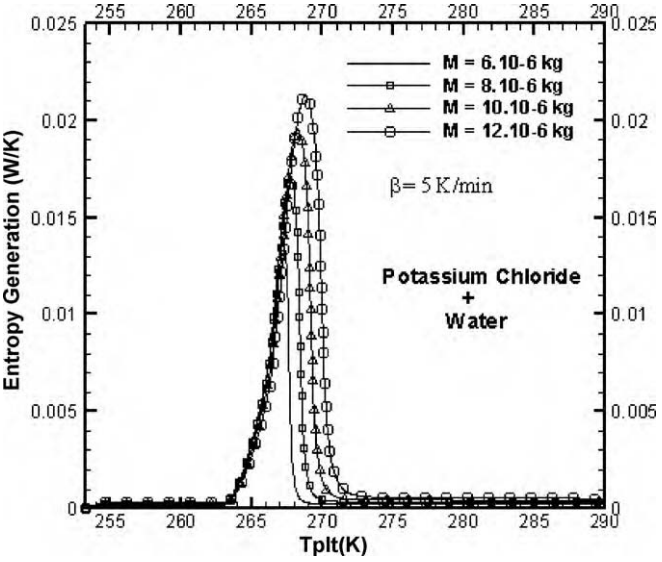

Fig. 7. Entropy generation versus T_{plt} for various cell masses.

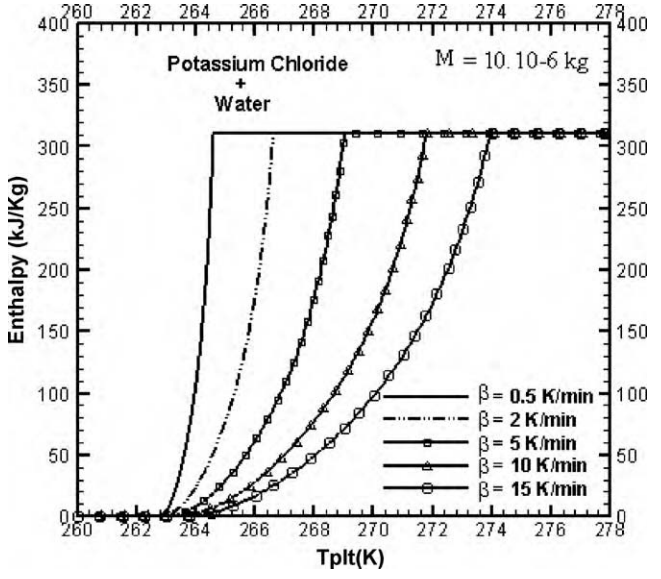

Fig. 8. Effect of the heating rate on the enthalpy change during the melting process.

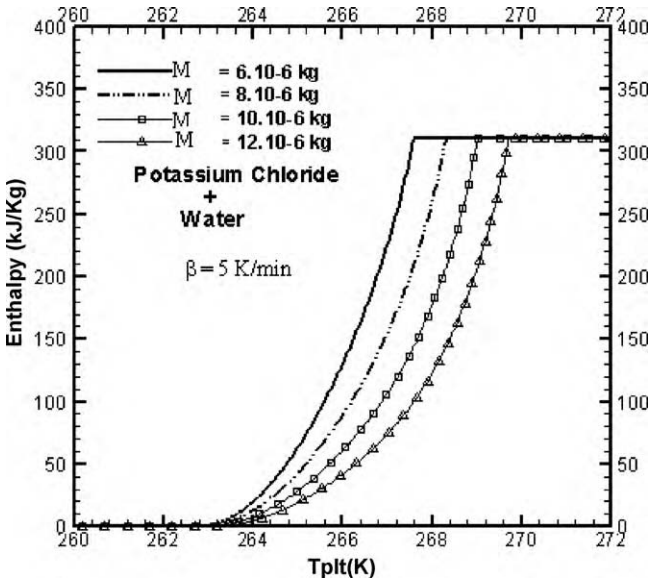

Fig. 9. Effect of the sample mass on the enthalpy change during the melting process.

change temperatures are very important since they decide the storage system's capacity, size and application range. When incorrect phase transition parameters are used in the PCM storage design, it will result in a lower than expected storage capacity.

6. Conclusions

A comprehensive thermodynamic analysis, incorporating the entropy generation in heat conduction, of a DSC sample phase change flow accompanied by melting process has been performed. The energy and entropy equations for two-dimensional transient thermal analyses with associated boundary and initial conditions have been solved numerically using a fixed grid numerical model with the finite control volume approach. This study helps to better understand the heat transfer processes during the DSC cell melting.

References

[1] A. Felix Regin, S.C. Solanki, J.S. Saini, Heat storage characteristics of thermal energy storage system using PCM capsules: a review, Renewable and Sustainable Energy Reviews 12 (2008) 2438–2458.
[2] I. Dincer, M.A. Rosen, Energetic, environment and economic aspects of thermal energy storage systems for cooling capacity, Applied Thermal Engineering 21 (2001) 1105–1117.
[3] A Abhat, Low temperature latent heat thermal energy storage: heat storage materials, Solar Energy 30 (1983) 313–332.
[4] G.A. Lane, Solar Heat Storage: Latent Heat Materials. Background and Scientific Principles, vol. I, CRC Press Inc., Florida, 1983.
[5] H.P. Garg, S.C. Mullick, A.K. Bhargava, Solar Thermal Energy Storage, D. Reidel Publishing Company, 1985, pp. 154–291.
[6] S.M. Husnain, Review on sustainable thermal energy storage technologies. Part 1. Heat storage materials and techniques, Energy Conversion and Management 39 (1998) 1127–1138.
[7] I. Dincer, A.R. Marc, Thermal Energy Storage, Wiley, New York, 2002.
[8] M.F. Mohammed, M.K. Amar, A.K.R. Siddique, A.H. Said, A review on phase change energy storage: materials and applications, Energy Conversion and Management 45 (2004) 1597–1615.
[9] B. Zalba, J.M. Martin, L.F. Cabeza, H. Mehling, Review on thermal energy storage with phase change: materials, heat transfer analysis and applications, Applied Thermal Engineering 23 (2003) 251–283.
[10] T. Kousksou, F. Strub, J. Castaing-Lasvignottes, A. Jamil, J.P. Bédécarrats, Second law analysis of latent thermal storage for solar system, Solar Energy Materials and Solar Cells 91 (2007) 1275–1281.
[11] B. He, V. Martin, F. Setterwall, Liquid–solid phase equilibrium study of tetradecane and hexadecane binary mixtures as phase change materials (PCMs) for comfort cooling storage, Fluid Phase Equilibria 212 (2003) 97–109.
[12] M. Merzlyakov, C. Schick, Thermal conductivity from dynamic response of DSC, Thermochimica Acta 377 (2001) 183–191.
[13] K. Kaneko, T. Koyaguchi, Simultaneous crystallization and melting at both the roof and floor of crustal magma chambers: experimental study using NH_4Cl–H_2O binary system, Journal of Volcanology and Geothermal Research 96 (2000) 161–174.
[14] T. Kousksou, A. Jamil, Y. Zeraouli, J.-P. Dumas, DSC study and computer modeling of the melting process in ice slurry, Thermochimica Acta 448 (2006) 123–129.
[15] T. Kousksou, A. Jamil, Y. Zeraouli, J.P. Dumas, Equilibrium liquidus temperatures of binary mixtures from differential scanning calorimetry, Chemical Engineering Science 62 (2007) 6516–6523.
[16] V.R. Voller, Implicit finite-difference solutions of the enthalpy formulation of Stefan problems, IMA Journal of Numerical Analysis 5 (1985) 201–214.
[17] V. Voller, C.R. Swaminathan, General source-based method for solidification phase change, Numerical Heat Transfer, Part B 19 (1991) 175–189.
[18] A. Jamil, T. Kousksou, Y. Zeraouli, S. Gibout, J.-P. Dumas, Simulation of the thermal transfer during an eutectic melting of a binary solution, Thermochimica Acta 441 (2006) 30–34.
[19] A. Bejan, Entropy Generation through Heat and Fluid Flow, Wiley, New York, 1982.
[20] G. Beggerow, Heats of mixing and solution, in: Landolt-Börnstein (Ed.), Numerical Data and Functional Relationships in Science and Technology – New Series, Group 4: Physical Chemistry, Band 2, Springer, Berlin, 1976.
[21] D.R. Lide, CRC Handbook of Chemistry and Physics: A Ready-Reference Book of Chemical and Physical Data, 84th ed., CRC Press, Boca Raton, 2004.
[22] V.M.M. Lobo, Handbook of Electrolyte Solutions, Elsevier, Amsterdam, 1989.